

## Bose-Einstein Condensation in $^{87}\text{Rb}$ : Characterization of the Brazilian Experiment

E. A. L. Henn,\* J. A. Seman, G. B. Seco, E. P. Olimpio, P. Castilho,  
G. Roati,† D. V. Magalhães, K. M. F. Magalhães, and V. S. Bagnato

*Instituto de Física de São Carlos, Universidade de São Paulo, Caixa Postal 369, 13560-970, São Carlos-SP, Brazil*

We describe the experimental apparatus and the methods to achieve Bose-Einstein condensation in  $^{87}\text{Rb}$  atoms. Atoms are first laser cooled in a standard double magneto-optical trap setup and then transferred into a QUIC trap. The system is brought to quantum degeneracy selectively removing the hottest atoms from the trap by radio-frequency radiation. We also present the main theoretical aspects of the Bose-Einstein condensation phenomena in atomic gases.

Keywords: Bose-Einstein condensation, quantum fluids, quantum phase transition, laser cooling and trapping, evaporative cooling.

### I. INTRODUCTION

Bose-Einstein condensation (BEC) is a phase transition which only can take place in bosonic systems. In last years, the study of BEC in atomic gases has become one of the most active research topics which links together different areas of physics. In quantum mechanics, BEC appears as a monochromatic giant matter wave [1]. In thermodynamics, it represents an important phase transition where a gas undergoes a change of observables, allowing the determination of a critical temperature [2]. In quantum field theory, BEC is an important demonstration of spontaneous symmetry break [3]. Condensed atoms are also an interesting window to the world of three body and many body interactions [4]. In statistical physics, BEC is a macroscopic occupation of a single quantum state [2]. Many other fields have advanced a lot from properties which are peculiar from BECs, and those include modern quantum computation among others.

Bose-Einstein Condensation became possible due to the great advances on laser cooling and magnetic trapping [5]. The ability to transfer light momenta to the atomic systems, in a controlled way, made possible the construction of atomic coolers, where atomic clouds at microkelvin of translational temperature are relatively easy to be obtained. Those samples are the starting point in the routes towards BEC.

A large number of atomic systems have been Bose condensed using a combination of techniques based on laser cooling, conservative trapping and evaporative cooling.  $\text{Rb}^{87}$  [6] was the first atomic species led to quantum degeneracy in 1995. Recently,  $\text{Yb}^{170}$  [7] and  $\text{K}^{39}$  [8] were also Bose condensed and now twelve different atomic species have already been Bose condensed (for the complete list prior to 2008 see Ref.[7]).

To obtain a sample Bose condensed it is necessary to build up density as well as lower the temperature in a way that the De Broglie wavelength becomes of the order of the mean distance between particles. In other words,  $n\lambda_{dB}^3 \geq 2.612$ , with

$\lambda_{dB} = h/\sqrt{2\pi mk_B T}$ , being the thermal de Broglie wavelength. A non homogeneous confining potential is a convenient way to reach such condition. Once there is a localized minimum for the potential, spatial compression is naturally achieved as the sample temperature lowers. One normally starts with a large number of atoms, held in a magneto-optical trap (MOT) and transfer the atomic cloud to a conservative trap. Following the conservative confinement, runaway evaporation allows to reach the necessary compromise between density and temperature.

To reach BEC in an atomic sample, a sequence of conditions has to be fulfilled. The preparation of the experimental system to have the necessary conditions is what determines the necessary time to bring a BEC experiment to function.

In a previous work [9] we have reported the observation of BEC in a gas of  $^{23}\text{Na}$  atoms. Our experimental apparatus had instabilities mainly related to technical limitations on the laser systems and mechanical layout, which prevent us to keep it running continuously. Indeed, this lack of reproducibility was not related to the atomic species itself. Experimental systems that produce BEC in  $^{23}\text{Na}$  atoms can be as well succeeded as any other system [10]. In our case, because of these technical reasons, we decided to move to a simpler system to observe and study BEC in a gas of  $^{87}\text{Rb}$  atoms.

In this paper we present a detailed description of the experimental setup that led us to observe BEC in a gas of  $^{87}\text{Rb}$  atoms. In fact, our system is very similar to the double-chamber systems for producing BEC, which is a very common setup with several variants. Nevertheless this is not the only way to design it: Zeeman slowed beams for loading the trap is another very common setup and both these configurations cover most of the experimental setups presently working. Special attention is given to provide basic concepts on the parameters evaluated in our system.

### II. EXPERIMENTAL SETUP

The conditions to reach BEC in an atomic sample require, usually, temperatures of the order of 100 nK and densities larger than  $10^{13} \text{ cm}^{-3}$ . The only technique known to be able to produce samples at these conditions is forced evaporative cooling. For this to be applied efficiently, it is needed

\*Electronic address: ehenn@ifsc.usp.br

†LENS and Dipartimento di Fisica, Università di Firenze, INFN and CNR-INFM, 50019 Sesto Fiorentino, Italy

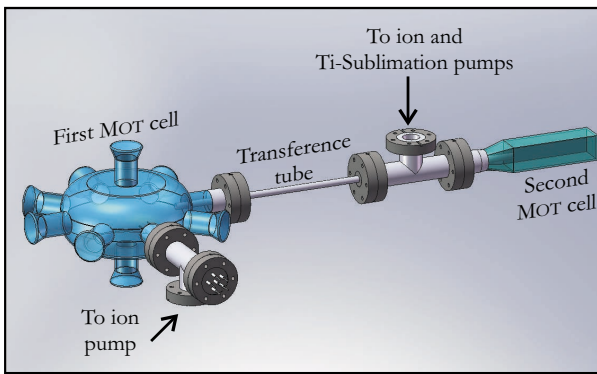


FIG. 1: Schematic view of the vacuum system showing the first and second chambers, the transference tube and the pumping ports.

a large number of trapped atoms in a conservative trap and a very low background pressure of untrapped atoms. These two conditions usually exclude each other unless one uses a slowed beam of atoms ending in a single chamber or a double-chamber configuration like ours.

The overall view of the vacuum system is shown in Fig. 1. The first chamber is made of Pyrex and contains ten windows and a vacuum port. Atoms collected in this first chamber are pushed through a narrow tube (4 mm wide and 40 cm long) to a second chamber. The connection of the first to the second chamber through this narrow tube allows a differential pressure of the order of  $10^2$ , which means keeping the second chamber at a very low pressure even when the first one is filled with *Rb*-vapor. The first chamber pressure ( $\sim 10^{-9}$  Torr) is kept by an ion pump, while the second chamber (with a pressure smaller than  $10^{-11}$  Torr) has a combination of ion and *Ti*-sublimation pumps. This second chamber is a Hellma cell also made of Pyrex, 6 cm long and with  $3 \times 3$  cm square cross-section.

We use *Rb*-metal dispensers [11] to coat the first cell walls with a *Rb* film. With the dispensers turned off we turn on six UV-LEDs [12] placed around the first cell. Each LED provides around 350 mW of light at 395 nm and acts like desorber for the *Rb* film. This *Rb* gas is collected in a MOT and up to  $10^9$  atoms are trapped in this way. As soon as the LEDs are turned off, the vapor is reabsorbed by the walls. This technique is known as *LIAD* and has been well described and characterized elsewhere [13].

The first MOT acts like a cold atom source for loading the second MOT. A continuous, 1 mW power push beam [14] transfers the atoms through the tube from one cell to the other, where they are captured. This second MOT loads up to  $10^9$  atoms in 35 s, that gives a mean flux of  $3 \times 10^7$  atoms/s.

Three different laser systems (TOPTICA DLX-110L) and several AOMs provide all necessary frequencies for the experiment. A layout of the laser system and the employed optics is presented in Fig. 2 and all the laser frequencies for this experiment are represented in Fig. 3. All the lasers are locked externally using saturated absorption technique, and all of them have linewidths better than 1 MHz. Optical isolators with suppression on the level of 60 dB prevent feedback from backre-

flection or backscattered light.

One laser system is fully dedicated to generate the cooling light for the first MOT. Only just before the beam expansion stage it is superimposed to the repumper light. The repumper frequency is generated by other laser system and after being produced, its light is divided and a small portion passes through an AOM, in order to generate one of the frequencies for the optical pumping process ( $5S^{1/2}(F=1) \rightarrow 5P^{3/2}(F=2)$ ). The major portion goes through an AOM in double-pass configuration, so the frequency of the laser can be tuned with minimal misalignment. This light is then almost equally divided, so part goes through a switching AOM, and then to be superimposed to the first MOT cooling light, and part is superimposed to the second MOT cooling light. The cooling light for the second MOT is generated by the third laser system. Like the repumper, a small portion is taken to generate the other optical pumping frequency ( $5S^{1/2}(F=2) \rightarrow 5P^{3/2}(F=2)$ ), then light goes through a double-pass AOM to allow frequency sweep with minimal misalignment for the optical molasses and imaging processes. Afterwards, another small portion is taken and goes through a switching AOM, then is divided and each of these is inserted into a PM optical fiber. These beams correspond to the push and imaging frequencies. The largest portion is then superimposed to the repumper light and both go through a switch AOM and a  $50\mu\text{m}$  pinhole, so we obtain 100mW of cooling light and 20mW of repumper light with a good gaussian spatial profile. This beam is then expanded and goes to the second MOT chamber. Both optical pumping frequencies are also superimposed and inserted into a PM optical fiber.

After the second MOT load is completed, the atoms are transferred into a full magnetic trap. Connecting these two stages, three different processes take place: MOT compression, optical molasses and spin-polarization. The first consists of changing the cooling laser frequency from its original  $\Delta = -20$  MHz detuning to  $\Delta = -50$  MHz for 6 ms. The rate of photon scattering is tremendously lowered and the atoms are compressed to the center of the trap. Following this, the magnetic field is turned off for 4 ms and sub-doppler cooling takes place. Finally, both cooling and repumper light are turned off, a homogeneous bias field is applied and a two-frequency light pulse pump all the atoms to the state  $|2, 2\rangle$ . This spin-polarization is needed because the pure magnetic trap holds only low-field-seeker states.

Once the cloud is spin-polarized, the magnetic field is turned on and the atoms are held in a spherical quadrupole with an axial gradient of 180 Gauss/cm which is raised to 600 Gauss/cm in 500 ms. The atoms are then transferred into a QUIC trap [15] in 800 ms.

The QUIC trap, shown in Fig.4(A), is composed of a quadrupole field generated by two coils operating in anti-Helmholtz configuration and an Ioffe coil. A current  $I_q$  through the quadrupole coils produces a spherical quadrupole trap. This trap can be converted into a QUIC by turning on the current  $I_{\text{Ioffe}}$ , which circulates through the Ioffe coil. On the sequence of profiles in Fig.4(B) one can observe the evolution of the magnetic potential as  $I_{\text{Ioffe}}$  increases. Increasing the current in the Ioffe coil, the mag-

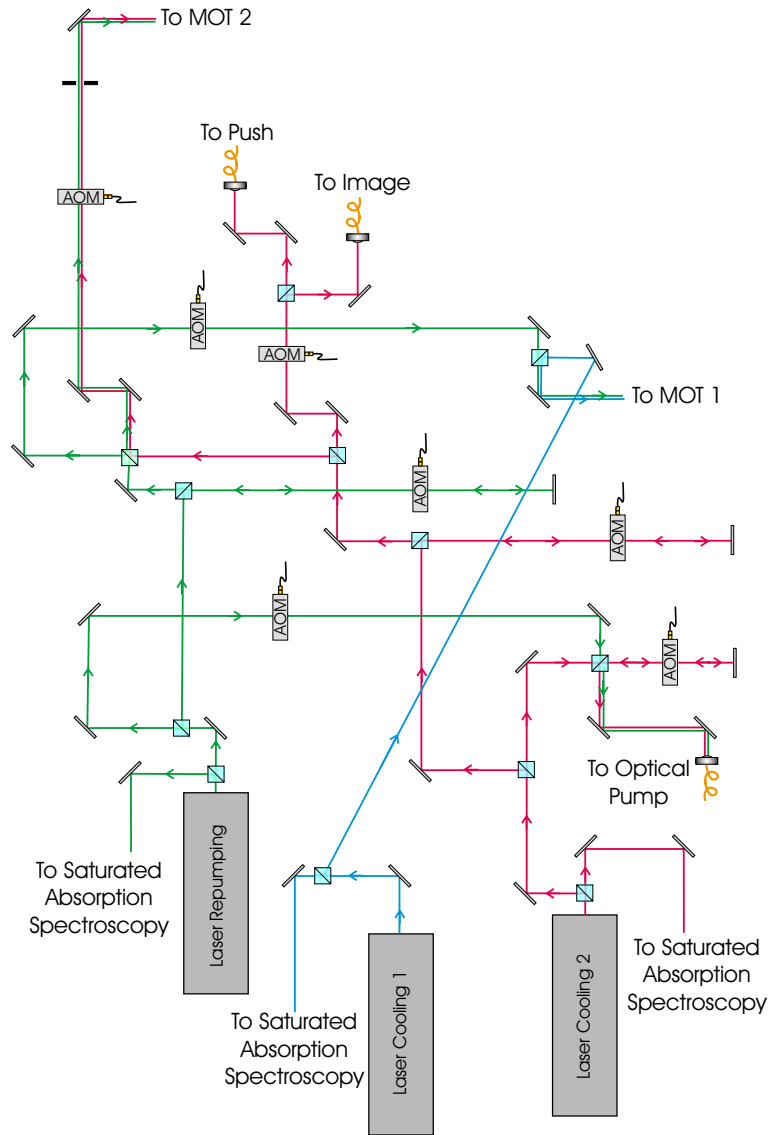


FIG. 2: Layout of the laser system, showing the three laser systems and main optical components. Waveplates and lenses are not shown for simplicity.

netic zero existent on the quadrupole center is progressively shifted towards the coil. At some current level, a second zero appears closer to the coil. At the final level of current (24 A) the two minima merge together, generating the quic trap with a bias field at the center. At the end stage, the overall trapping potential felt by weak-field-seeker atoms is given by  $U(x, y, z) = U_0 + \frac{1}{2}m(\omega_x^2 x^2 + \omega_y^2 y^2 + \omega_z^2 z^2)$ , where  $\omega_x \sim \omega_y = 9\omega_0$  and  $\omega_z \sim \omega_0$ , with  $\omega_0 \sim 23\text{Hz}$ . Such a large anisotropy produces a cigar-shaped atomic cloud.

Once atoms are transferred to the QUIC, evaporation is used to obtain lower temperatures. Evaporation is done using an antenna irradiating Radio-Frequency (RF), that produces a spin-flip transition, transforming trappable into untrappable atoms. For a given value of RF only atoms at specific magnetic field amplitude are affected and ejected from the trap. Sweeping from a high to a low value of frequency we can

force evaporation while colder atoms accumulate at the trap center. If this sweeping of RF is performed in an optimized rate, a great increase of phase-space density is achieved. The RF was scanned from 16 MHz down to the point where BEC takes place ( $\sim 1.6\text{MHz}$ ). To optimize the RF sweeping, one must investigate the best time-dependence for the frequency. Fig. 5(A) shows the optimized ramp for our experiment and Fig. 5(B) exhibits a sequence of Time-of-Flight absorption measurements showing a considerably degree of cooling and phase-space increasing.

The cooling process on the atomic cloud is observed through absorption of a probe laser beam resonant with the  $F = 2 \rightarrow F' = 3$  transition. The propagation of the probe beam on the  $y$ -direction, produces a two-dimensional intensity profile  $I(x, z) = I_0 \exp[-\alpha(x, z)]$ , where  $\alpha(x, z) = -\sigma \int n(x, y, z) dy$  is the optical density of the sample and

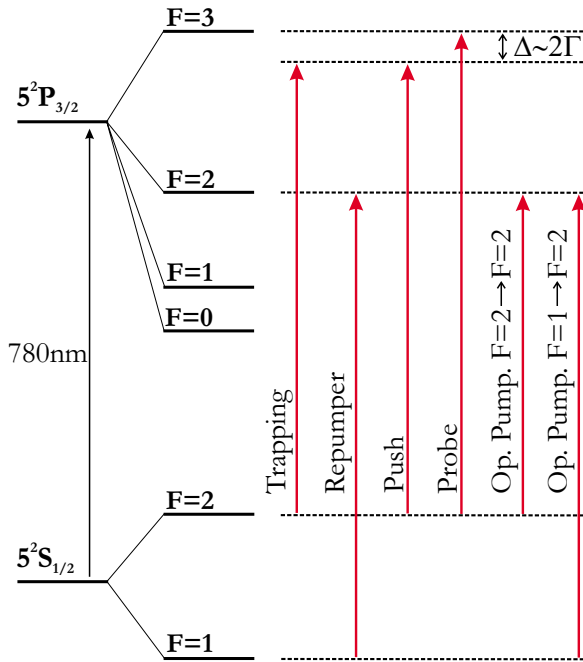


FIG. 3:  $^{87}\text{Rb}$   $D_2$  transition hyperfine structure, with frequency splittings between the hyperfine energy levels. The frequencies used in the experiment are shown.

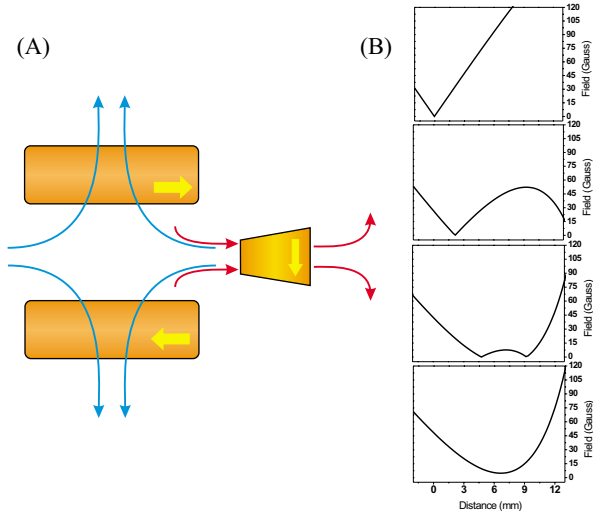


FIG. 4: (A) Schematic configuration of coils of the QUIC trap and (B) a sequence of magnetic field profiles as the Ioffe current is increased.

$n(x, y, z)$  its density. An integration of  $\alpha(x, z)$  along the  $xz$  plane provides the total number of atoms in the sample:

$$N = \frac{1}{\sigma} \int \alpha(x, z) dx dz \quad (1)$$

where  $\sigma$  is the absorption cross section for a near resonant light. For the transition  $5S^{1/2} \rightarrow 5P^{3/2}$ ,  $\sigma \approx \sigma_0 / \left[ 1 + 4 \left( \frac{\Delta}{\Gamma} \right)^2 \right]$  with  $\sigma_0 = 1.4 \times 10^{-9} \text{cm}^2$  [16].

Figure 6 summarizes the techniques used in this process and all the related time scales.

### III. OBSERVING BOSE-EINSTEIN CONDENSATION

To observe BEC in the sample, it is necessary an efficient evaporative cooling. To achieve efficient evaporation the first requirement is that the rate of elastic collisions,  $\gamma = n\sigma_{el}v$ , which are responsible for the rethermalization of the sample, overcomes the rate of inelastic collisions, which remove atoms from the trap, where  $n$  is the particle density,  $\sigma_{el}$  is the elastic collision cross-section, and  $v$  denotes the average thermal velocity [17]. Then, to well succeed in evaporation it is necessary to have  $\gamma$  overcoming the loss rate during the whole process, even with the decreasing in the atomic number. The important parameter to be observed is the phase-space-density ( $D$ ), or the number of atoms per cubic de Broglie wavelength. One can calculate  $D$  as  $D = n\lambda_D^3$ , which for  $^{87}\text{Rb}$  can be expressed as

$$D = \frac{6.67n}{T^{3/2}} 10^{-24} \quad (2)$$

where  $n$  is expressed as  $\text{particles}/\text{cm}^3$  and  $T$  in Kelvin. For a harmonic trap, density varies with temperature as  $n \propto N/T^{3/2}$ , such that  $D \propto N/T^3$ . An efficient evaporation demands that  $T$  decreases faster than  $N$ , to increase  $D$ . One can show that the evolution of  $N$  with  $T$  must obey a relation like  $N \propto T^s$  with  $s \leq 1$  to fulfill the conditions for an efficient runaway evaporation [18]. Smaller the value of  $s$ , greater evaporation efficiency is achieved. For a harmonic trap, it is shown that the critical temperature  $T_c$  is related to the number of particles by  $k_B T_c = 0.941\omega N^{1/3}$  [19]. This relation sets, in some sense, the critical line for the observation of BEC.

The graph shown in Fig. 7 represents the route followed by the number of trapped particles as a function of temperature in our experiment. The first fact to be observed is that  $s \approx 0.73 \pm 0.04$ , showing the occurrence of runaway evaporation. For a temperature around 160 nK the quantum degeneracy border is crossed and condensation is observed, with a number of about  $7 \times 10^5$  particles. At the critical temperature, the peak density of atoms corresponds to  $4 \times 10^{13} \text{cm}^{-3}$ . Pure condensates containing  $2 \times 10^5$  atoms are observed.

Besides reaching  $D \geq 2.6$ , there are a few signatures that happen together with the occurrence of BEC. A dramatic change in the shape of the spatial density profile, as observed by absorption, is the most important signature of BEC. As recorded by our CCD camera, the point just below BEC is shown in Fig. 8(A), together with the cut of the density profile (Fig. 8(B)). At condensation, the traditional Gaussian density profile for the trapped cloud is suddenly changed by the appearance of a peak, with a great deviation. The observed peak has a parabolic shape and it is due to the dominance of interactions in this sample at the existent conditions of density and temperature.

To explain this profile, we start considering the Gross-Pitaevskii equation for one particle in the condensate

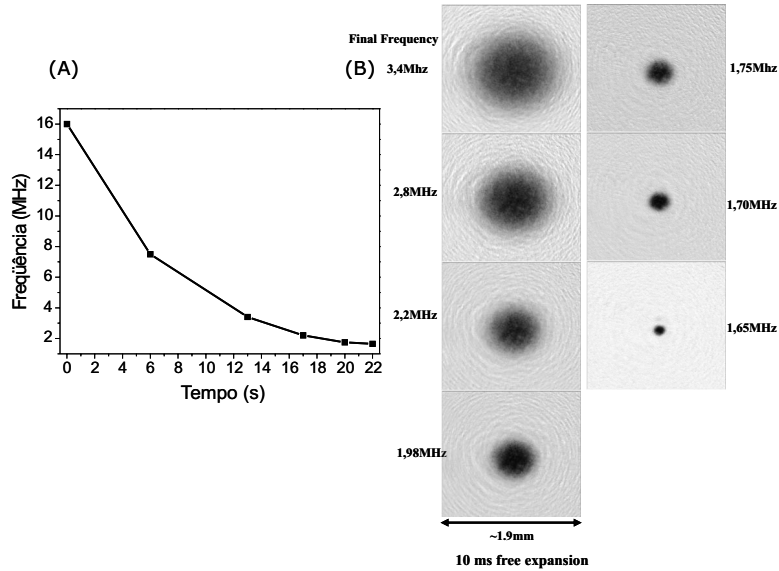


FIG. 5: (A) Evaporation frequency as a function of time, and (B) sequence of 10 ms time-of-flight absorption measurements showing the cloud evolution as the evaporation frequency is decreased.

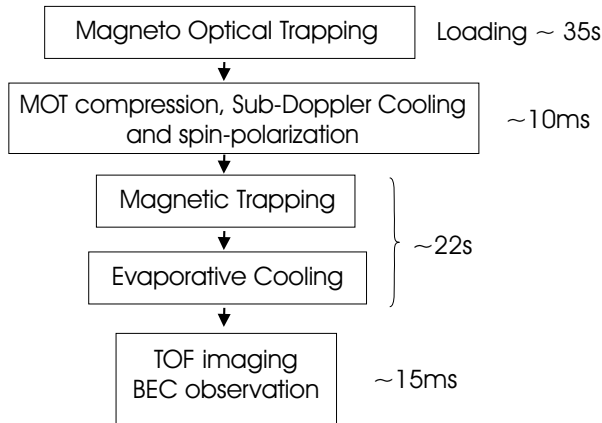


FIG. 6: Experimental and time sequence of the experiment.

$$\left\{ -\frac{\hbar^2}{2M} \nabla^2 + U(r) + g|\Psi|^2 \right\} \Psi = \mu\Psi, \quad (3)$$

which is basically the Schrödinger equation with an extra term, proportional to  $|\Psi|^2$ , from interactions. The coupling constant is

$$g = \frac{4\pi\hbar^2 Na}{M}, \quad (4)$$

with  $a$  being the s-wave scattering length. The chemical potential  $\mu$  represents the energy of an individual atom in the presence of all the others.

At ultra-low temperatures, the Gross-Pitaevskii equation can be approximated by an algebraic equation when interaction is the dominant term. This is the so-called Thomas-Fermi

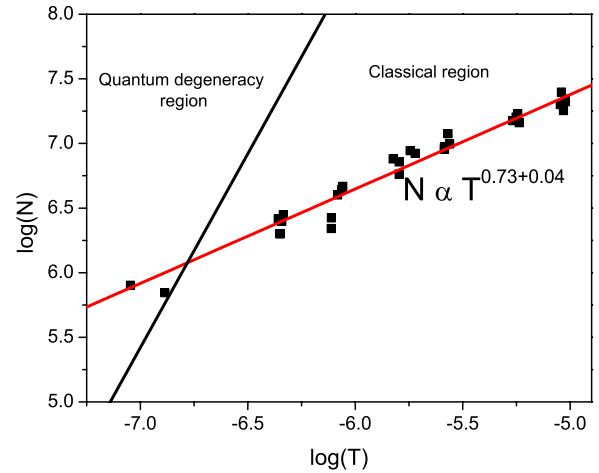


FIG. 7: Evolution of the number of trapped particles as the temperature of the sample decreases, showing an efficient evaporative cooling and the crossing of the transition boundary.

regime, where the kinetic energy term can be neglected when compared to the others. In this case

$$\{U(r) + g|\Psi|^2\} \Psi = \mu\Psi, \quad (5)$$

such that for the region where  $\Psi \neq 0$ ,

$$|\Psi|^2 = \frac{\mu - U(r)}{g}, \quad (6)$$

since  $N|\Psi|^2 = n(\vec{r})$ , for  $U(r) = \frac{1}{2}m(\omega_x^2 x^2 + \omega_y^2 y^2 + \omega_z^2 z^2)$ , we have



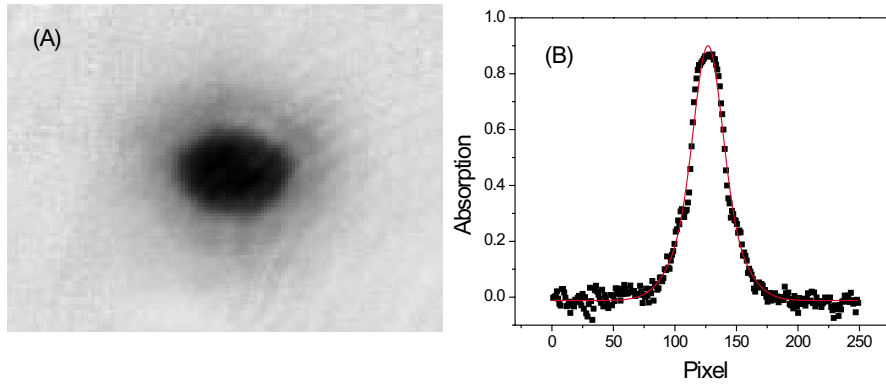


FIG. 8: Onset of condensation just below critical temperature, showing (A) the absorption CCD camera picture and (B) absorption profile showing the double spatial distribution, which is well fitted by a combination of a gaussian profile for the thermal cloud and an inverted parabola profile for the condensed cloud.

$$n(r) = n_0 \left\{ 1 - \left[ \left( \frac{x}{R_x} \right)^2 + \left( \frac{y}{R_y} \right)^2 + \left( \frac{z}{R_z} \right)^2 \right] \right\}, \quad (7)$$

where  $n_0$  is the atomic density at the center of the condensate and  $R_i$  is determined as  $\frac{1}{2}m\omega_i^2 R_i^2 = \mu$ , for  $i = x, y, z$ .

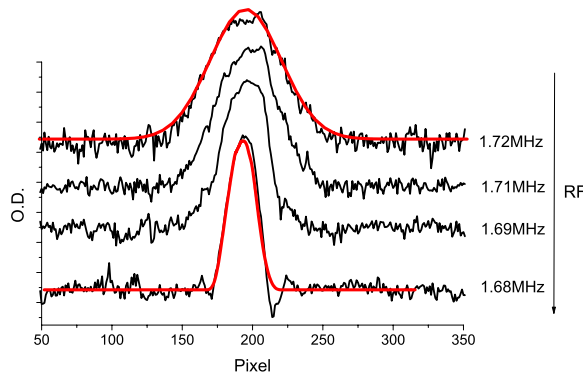


FIG. 9: Sequence of images showing the appearance of BEC as the evaporation Radio-Frequency is lowered. The first image is well fitted by a gaussian profile as it is above the transition. The last image is fitted by an inverted parabola characteristic of the Thomas-Fermi profile.

In Fig. 9, we observe a sequence of images going from a pure thermal cloud until an almost pure sample of condensate atoms. Observe that while the thermal cloud (non-condensate fraction) is well fitted by a Gaussian function, the condensate is well fitted by the inverted parabola.

The combination of fitting within the density profile, allows separating the condensate fraction. On Fig. 10, the condensate fraction as a function of temperature is presented. For a repulsive harmonic trapped gas, a first order approximation predicts that the expected fraction of condensate atoms is given by  $\frac{N_0}{N} = 1 - \left( \frac{T}{T_c} \right)^3 - 4 \frac{a}{\lambda_{dB}} \left( \frac{T}{T_c} \right)^{7/2}$  [19], applying this relation

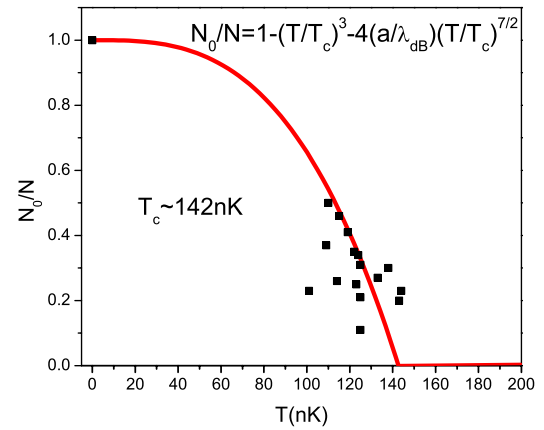


FIG. 10: Condensate fraction as a function of the temperature of the sample and theoretical fitting from which we obtain 142nK for the critical temperature.

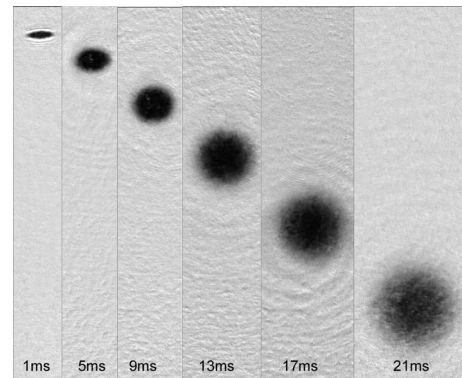


FIG. 11: Expansion of a thermal cloud as a function of time showing its evolution to isotropy.

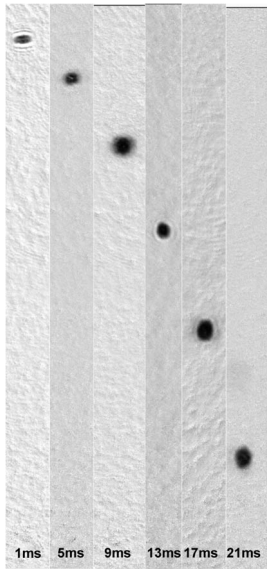


FIG. 12: Expansion of a BEC as a function of time showing the typical inversion of aspect ratio of the quantum cloud.

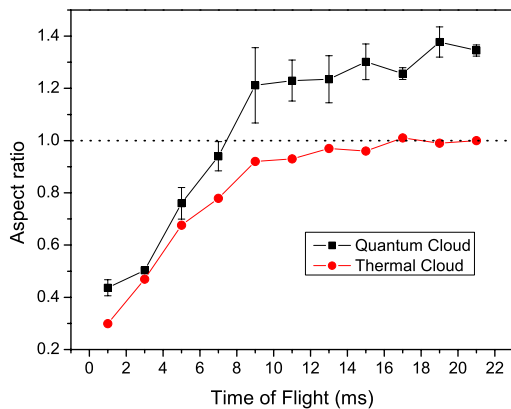


FIG. 13: Aspect ratio for a classical (circles) and a quantum (squares) cloud as a function of the expansion time.

to our data, we observed a good adjustment with  $\frac{a}{\lambda_{dB}} \approx 0.01$ . For  $^{87}\text{Rb}$ ,  $a \approx 5 \text{ nm}$  and at  $T \approx 160 \text{ nK}$ ,  $\lambda_{dB} \approx 0.5 \mu\text{m}$ , showing good agreement in first order correction.

The asymmetric velocity distribution of the expanded cloud is another clear indication of BEC. Before reaching BEC (above  $T_c$ ), the cloud expands spherically, as expected from thermal atoms. An example of such expansion is shown on Fig. 11. We start having the aspect ratio between the two dimensions of the cloud as the ratio of the trap frequencies. As the cloud expands it turns into a spherical expanding cloud. On the other hand, for a condensate cloud of atoms, during the expansion, the cloud suffers an inversion of the aspect ratio, as presented in Fig. 12. For the condensate, as the expansion takes place, the conversion of interaction energy into motion does not follow the thermal equilibrium arguments for the thermal clouds. A better comparison can be made observing Fig. 13, where the numerical aspect ratio for a thermal cloud and for a condensate are plotted as a function of the expansion time. At the beginning, the aspect ratio for both clouds evolves in a similar way. Sooner the quantum gas and the thermal gas start to deviate from each other. After a time in which the thermal cloud starts to expand isotropically (aspect ratio equal to 1) the condensate shows the inversion ratio and the aspect ratio becomes larger than unity.

The observation of the aspect ratio inversion is an undoubtedly signature for BEC, which could not take place otherwise.

#### IV. CONCLUSIONS

In this paper we have described step by step the experimental realization of Bose-Einstein Condensation for a sample of  $^{87}\text{Rb}$  atoms held in a QUIC-type trap. The typical number of atoms in the BEC is  $2 \times 10^5$  and the critical temperature  $T_c$  is about  $100 \text{ nK}$ .

We have started to use the condensate sample to pursue studies involving different aspects of the condensate, like non-zero temperature corrections and topological-like excitations. The experimental observation of these excitations will be published in future works [20].

- 
- [1] M.-O. Mewes, M. R. Andrews, D. M. Kurn, D. S. Durfee, C. G. Townsend, and W. Ketterle, *Phys. Rev. Lett.* **78**, 582 (1997).
  - [2] K. Huang, *Introduction to Statistical Physics* (Taylor & Francis, New York, 2001).
  - [3] J. I. Kapusta, *Phys. Rev. D* **24**, 426 (1981).
  - [4] I. Bloch, J. Dalibard, and W. Zwerger, arXiv:0704.3011v2 [cond-mat.other] 17 Oct 2007.
  - [5] H. J. Metcalf, and P. van der Straten, *J. Opt. Soc. Am. B* **20**, 887 (2003).
  - [6] M. H. Anderson, J. R. Ensher, M. R. Matthews, C. E. Wieman, and E. A. Cornell, *Science* **269**, 198 (1995).
  - [7] T. Fukuhara, S. Sugawa, and Y. Takahashi, *Phys. Rev. A* **76**, 051604(R) (2007).
  - [8] G. Roati, M. Zaccanti, C. D'Errico, J. Catani, M. Modugno, A. Simoni, M. Inguscio, and G. Modugno, *Phys. Rev. Lett.* **99**, 010403 (2007).
  - [9] K. M. F. Magalhães, S. R. Muniz, E. A. L. Henn, R. R. Silva, L. G. Marcassa, and V.S. Bagnato, *Laser Phys. Lett.* **2**, 214 (2005).
  - [10] E. W. Streed, A. P. Chikkatur, T. L. Gustavson, M. Boyd, Y. Torii, D. Schneble, G. K. Campbell, D. E. Pritchard, and W. Ketterle, *Rev. Sci. Instrum.* **77**, 023106 (2006).
  - [11] Alkali Metal Dispensers - SAES getters.
  - [12] Ultraviolet Edixeon, model EDEV-3LA1.
  - [13] C. Klempt, T. van Zoest, T. Henninger, O. Topic, E. Rasel, W. Ertmer, and J. Arlt, *Phys. Rev. A* **73**, 013410 (2006).
  - [14] L. Cacciapuoti, A. Castrillo, M. de Angelis, and G. M. Tino,

- Eur. Phys. J. D **15**, 245 (2001).
- [15] T. Esslinger, I. Bloch, and T. W. Hänsch, Phys. Rev. A, **58**, R2664 (1998).
- [16] D. A. Steck, *Rubidium 87 D Line Data*, <http://steck.us/alkalidata> (2003)
- [17] W. Ketterle, and N. J. van Druten, in *Advances in Atomic, Molecular and Optical Physics*, edited by B. Bederson and H. Walther (Academic Press, San Diego, 1996), No. 36.
- [18] J. E. Lye, C. S. Fletcher, U. Kallman, H.-A. Bachor, and J. D. Close, J. Opt. B: Quantum Semiclass. Opt. **4**, 57 (2002).
- [19] V. Bagnato, D. E. Pritchard, and D. Kleppner Phys. Rev. A **35**, 4354 (1987).
- [20] E. A. L. Henn, J. A. Seman, G. Roati, P. Castilho, E. P. Olimpio, K. M. F. Magalhães, and V. S. Bagnato, *Vortex Formation by an off-axis oscillating spherical quadrupole field in a Bose-Einstein condensate* - manuscript in preparation (2008)